Plasmonic ruler on field-effect devices for kinase drug discovery applications

Nikhil Bhalla[1], Nello Formisano[1], Anna Miodek[1], Aditya Jain[2], Mirella Di Lorenzo[3], Giordano Pula[4], Pedro Estrela[1,*]

[1]Department of Electronic & Electrical Engineering, University of Bath, Bath BA2 7AY, United Kingdom; Email: N.Bhalla@bath.ac.uk, N.Fornisano@bath.ac.uk, A.Miodek@bath.ac.uk, P.Estrela@bath.ac.uk

[2]Department of Physics and Astronomy, Iowa State University, Ames, Iowa 50011, United States of America; Email: ajain17@iastate.edu

[3]Department of Chemical Engineering, University of Bath, Bath BA2 7AY, United Kingdom; Email: M.Di.Lorenzo@bath.ac.uk

[4]Department of Pharmacy & Pharmacology, University of Bath, Bath BA2 7AY, United Kingdom; Email: G.Pula@bath.ac.uk

*Corresponding author: Department of Electronic & Electrical Engineering,
University of Bath,
Claverton Down, Bath, BA2 7AY, United Kingdom
E-mail: P.Estrela@bath.ac.uk
Phone: +44-1225-386324

Abstract

Protein kinases are cellular switches that mediate phosphorylation of proteins. Abnormal phosphorylation of proteins is associated with lethal diseases such as cancer. In the pharmaceutical industry, protein kinases have become an important class of drug targets. This study reports a versatile approach for the detection of protein phosphorylation. The change in charge of the myelin basic protein upon phosphorylation by the protein kinase C-alpha (PKC-α) in the presence of adenosine 5'-[γ-thio] triphosphate (ATP-S) was detected on gold metal–insulator–semiconductor (Au-MIS) capacitor structures. Gold nanoparticles (AuNPs) can then be attached to the thio-phosphorylated proteins, forming a Au-film/AuNP plasmonic couple. This was detected by a localized surface plasmon resonance (LSPR) technique

alongside MIS capacitance. All reactions were validated using surface plasmon resonance technique and the interaction of AuNPs with the thio-phosphorylated proteins quantified by quartz crystal microbalance. The plasmonic coupling was also visualized by simulations using finite element analysis. The use of this approach in drug discovery applications was demonstrated by evaluating the response in the presence of a known inhibitor of PKC-α kinase. LSPR and MIS on a single platform act as a cross check mechanism for validating kinase activity and make the system robust to test novel inhibitors.

Introduction

Kinase mediated phosphorylation is one of the major post translational modifications of the proteins essential for the regulation of various cellular functions, such as cell cycle, motility, metabolism or genetic expression (Cohen 2002; Noble et al. 2004; Overington et al. 2006; Weller 1979). Abnormal phosphorylation of proteins is associated with etiology of fatal diseases such as cancer (Chakraborty et al. 2014; Viatour et al. 2005), cardiovascular (Honda et al. 1998; Liu and Molkentin 2011), spinal (de Laat et al. 2014; Kyriakis 2014) and neural disorders (Abeliovich 2014; Buee et al. 2000). In this perspective the development of inhibitors for kinases could serve as powerful drugs for a specific disease associated with phosphorylation. Kinases catalyse the addition of phosphoryl group to the serine, threonine and tyrosine amino acids in the presence of a phosphate source, like ATP, where the γ-phosphoryl group is transferred to the amino acid (Cohen 1988; Kerman and Kraatz 2009). Upon phosphorylation, there is an addition of negative charge on the protein and a release of proton, while ATP is converted into ADP (Lindsay 2012). Electrochemical (Kerman et al. 2007; Kerman and Kraatz 2009; Kerman et al. 2008) and optical techniques (Li et al. 2010) to detect protein phosphorylation have proved to be highly sensitive, selective, less time consuming and more cost effective than the conventional techniques such as mass spectroscopy (Kruger et al. 2006; Rusinova et al. 2009), radioactive isotope (Steen et al. 2005) and antibody labelling assay (Morgan et al. 2004). Recently, we detected the release of proton associated with phosphorylation reaction on electrolyte-insulator-semiconductor (EIS) structures (Bhalla et al. 2014) and EIS structures couple with plasmonic effects (Bhalla et al. 2015). In the current study, on the other hand, we detect the phosphorylation of proteins by identifying the change in the charge of the myelin basic protein (MBP) with the use of metal (gold)–insulator–semiconductor (MIS) capacitor structures (Figure 1). We employ the use of

5'-[γ-thio] triphosphate (ATP-S) where the γ-phosphoryl group linked with the sulphide group enables the attachment of gold nanoparticles (AuNPs) to the thio-phosphorylated substrate and forms Au-film and AuNP plasmonic couple. This plasmonic coupling results in the shift of resonance wavelength of gold. It also precisely quantifies the distance between the sensor film and the NP by slightly modifying the decay constant of plasmonic ruler equation demonstrated for AuNP-AuNP pair (Jain et al. 2007a). A practical application of plasmonic rulers as a complementary validation on the MIS sensing platform that distinguishes phosphorylated proteins from the un-phosphorylated ones was therefore investigated. For validation purposes, all the reaction steps were followed using automated surface plasmon resonance (SPR) in real time on gold chips. This allowed: 1) quantification of protein surface coverage; 2) rough estimation of the percentage of total sites that get phosphorylated; 3) to determine the effect of NP binding on the thio-phosphorylated gold substrates. Quartz crystal microbalance (QCM) measurements were also conducted to quantify the nanoparticles and co-relate with the thio-phosphorylated sites estimated by SPR on the gold surface. Moreover this work emphasises the need to converge multiple sensing technologies in a single platform to analyse multiple parameters of a chemical reaction in real time for robust verification of biochemical processes. Multiple techniques incorporated on a single platform could potentially save time and cost of analysis for authenticating a chemical reaction. For instance, in this study we unveil the capabilities of AuNPs to combine multiple sensing techniques that enable simultaneous localized surface plasmon resonance (LSPR) and MIS validation of protein phosphorylation. In addition, the use of AuNPs massively amplifies the angle resolved sensitivity of SPR setup. Most significant advantage of this methodology is that the advances in the microelectronics can easily replicate these techniques in an array format for high throughput analysis of kinase assays (Liu et al. 2014). This would ultimately speed up the development of novel kinase inhibitors and activators that are currently being explored in pharmaceutical research and drug discovery. In addition, it may have important applications for the future use of nanoparticle-based technologies in drug discovery.

Materials and Methods

Reagents

All chemicals were of analytical grade and used as received, unless otherwise specified. All aqueous solutions were made with ionised water, 18.2 MΩ cm, with a Pyrogard filter

(Millipore, USA). Tris base, magnesium chloride, sodium chloride, acetone, ammonium hydroxide, hydrochloric acid, hydrogen peroxide, mercaptoundecanoic acid (MUA), mercaptohexanol (MCH), ethanolamine, ethanol, NHS (N-hydroxysuccinimide) , EDC (ethyl-dimethylaminopropyl carbodiimide), PKC-α kinase inhibitor GF 109203X, adenosine tri-phosphate (ATP) Gold nanoparticles, 20 nm average spherical diameter, in 0.1 mM PBS were purchased from Sigma-Aldrich. Dephosphorylated myelin basic protein (MBP), purified from bovine brain using fast protein liquid chromatography (FPLC), was purchased from Millipore. PKC-α human recombinant kinase produced in Sf9, was procured from ProSec-Tray TechnoGene Ltd. PKC lipid activator cocktail was obtained from Millipore. Polyclonal phospho-(Ser) PKC substrate antibody was purchased from Cell Signaling Technology.

Instrumentation

Capacitance–voltage (*C–V*) measurements of the electrolyte–metal–insulator–semiconductor structures were performed using a CompactStat potentiostat (Ivium Technologies, The Netherlands). LSPR was measured using an in-house built system with discrete components, all bought from Ocean Optics (USA). The system had 3 parts: reflection probe (R400-7-UV-VIS) with both detector and light source, connected to Tungsten Halogen (Source LS-1-LL) and a spectroscope (USB4000-UV-VIS-ES). The data was obtained through absorption mode on a cross platform spectroscopy operation software (SPECTRASUITE) provided by Ocean Optics. SPR measurements were done on SR7000DC SPR System purchased from Reichert Technologies (USA). QCM was performed on JLMQ USB Interface and recorded with a Multisense analyzer purchased from JLM Innovation (Germany).

Substrate preparation

MIS capacitance and LSPR were carried out on in-laboratory prepared substrates. Ten nanometre of chromium, an adhesion layer for gold, and 100 nm of gold were deposited by thermal evaporation on Si_3N_4 substrates. Prior to this, the Si_3N_4 wafer was firstly rinsed with ultra-pure deionised (DI) water and then immersed in 1:1:5 solution of NH_4OH:H_2O_2:DI at 80 °C for 10 min to remove organic contaminants. Afterwards, to remove inorganic contaminants, the wafer was soaked in 1:1:6 solution of HCl:H_2O_2:DI at 80 °C for 10 min; finally the wafer was rinsed with DI. Si_3N_4 was deposited by plasma-enhanced chemical vapour deposition (PECVD) onto 4-inch n-type Si wafers with 50 nm of SiO_2. After cleaning the wafer, 100 nm aluminium was physically deposited on the back of the Si wafer to serve as an ohmic back-contact using an Edwards (UK) e-beam evaporator. The final structure from

bottom to top was Al-Si–SiO_2–Si_3N_4-Au. The wafer was sandwiched between a teflon well with an o-ring and a conductive plate (copper), so that the aluminium coated side of the wafer sits on the lower conductive plate. This formed a planar gold well with 19.64 mm^2 interrogation area for the reaction defined by the size of the o-ring (5 mm diameter). 50 nm gold coated SPR gold chips, supplied from Reichert Technologies were used for studying the reaction on SPR. Prior to their use, these chips were cleaned using piranha solution (3:1 H_2SO_4:H_2O_2) and rinsed thoroughly with DI. 10 MHz QCM crystals were purchased from JLM innovation and were given a stringent acetone wash before use.

Bio-functionalization of Au substrates

The dried and cleaned Au substrates were incubated in MUA, 1 mM and MCH, 1 mM in a ratio of 1:9 for 18 hours in ethanol. The carboxyl groups were converted to amine-reactive NHS esters for bio-conjugation using 10 mM EDC/NHS in a ratio of 4:1. 156 μM myelin basic protein (MBP) was dispensed on the Au surface for 15 min, enabling the amino groups of MBP to attach to the ester group of carboxyl EDC/NHS activated complex. The unreacted MUA sites were blocked by incubating the sample in ethanolamine, 1 mM, in Tris buffer pH 7.5 for 10-12 min.

Protein thio-phosphorylation reaction on Au surface

PKC-α protein kinase was selected for the study in this work. Myelin basic protein is a well-known substrate of PKC-α and thio-phosphorylation of MBP by PKC-α kinase has been reported in association with multiple sclerosis. Thio-phosphorylation of MBP was carried out in a buffer with 0.2 mM Tris base, pH 7.4, 6 mM NaCl and 0.4 mM $MgCl_2$. The reaction was initiated by exposing MBP to 1 μM ATP-S, 40 mU/ μl of PKC-α and 1.25 μl/U of PKC lipid kinase activator containing 0.5 mg/ml phosphatidylserine and 0.05 mg/ml diacyglycerol in 20 mM MOPS (pH 7.2), 25 mM β-glycerol phosphate, 1 mM sodium orthovanadate, 1 mM dithiothretiol and 1 mM $CaCl_2$. After thio-phosphorylation the substrates were exposed to 100 μl of 20 nm AuNPs 0.1 mM in PBS. Two sets of control reactions were performed, one without PKC lipid activator and another with 0.1 μM PKC kinase inhibitor (GF 109203X). In addition a third control reaction i.e. phosphorylation in the presence of 1 μM ATP instead of ATP-S was done to check the non-specific attachment of AuNPs to the proteins.

MIS Capacitance and LSPR Measurements

A conventional three-electrode electrochemical setup was employed with an Ag/AgCl reference electrode immersed in the electrolyte *via* a salt bridge used to apply the gate voltage

and a Pt counter electrode. During the measurements, the gate voltage (V_g, applied between the reference electrode and the Al back-contact) was varied between -2 and +2 V, superimposed with a small ac signal of 10 mV at 1 kHz. The first measurement for the reaction was taken after protein immobilization, i.e. before the start of phosphorylation process. After adding the kinase, ATP and kinase activator, the activity of the reaction was studied by recording the *C–V* characteristics every 2 min for 8 min. Finally, the measurement was taken at 20 min after the start of the phosphorylation reaction. At this instance gold nanoparticles were added and after 10 min a reading was taken before washing with the reaction buffer. After this the sample was allowed to stabilize and two readings were taken at a gap of 10 min. In the control reactions, *C–V* measurements were taken at similar time intervals. Each experiment was repeated at least six times and the reported data correspond to the average values. The maximum observed value of the capacitance, C_{max}, which corresponds to $C_{dielectric}$ (capacitance of the silicon nitride/silicon dioxide dielectric layers) does not vary more than 3% from curve to curve. Therefore the curves have been normalised to C_{max} for the ease of comparison. LSPR measurements were taken on the same sample simultaneously at two instances, first after thio-phosphorylation but before adding gold nanoparticles and second after adding nanoparticles. The readings were recorded by the Spectrasuite software via LSPR system as described above.

SPR and QCM Measurements

SPR measurements were done using a Reichert SPR 7000DC dual channel flow spectrometer at 25 °C. The concentrations of protein, kinase, ATP-S, inhibitor and other bio-functionalization reagents were the same as described above. All buffers, namely Tris buffer (same as described above) and PBS 0.1 mM, pH 7.5 were filtered through 0.2 μm filters and degassed for 2 hours by sonication. The MUA/MCH modified Au chips were kept in running Tris buffer at a flow of 25 μl/min until a stable baseline was achieved. Then the surface was activated with EDC/NHS for 5 minutes and exposed to the proteins for 10 minutes. After this, ethanolamine was injected for 10 minutes. Between each step washing of the surface was performed using the running buffer. Subsequently thio-phosphorylation was done in the presence of ATP-S, kinase activator and kinase and then the surface was washed with the running buffer after 15 minutes of incubation. Then, the running buffer was changed to 0.1 mM PBS since the gold nanoparticles were prepared in 0.1 mM PBS and the thio-phosphorylated chips were kept in the running buffer at 35 μl/min until stability of baseline was obtained. Finally gold nanoparticles were injected for 15 min followed by a washing step

with PBS buffer to remove non bounded residues. The experiments were repeated 8 times to check the reproducibility and average values are reported here. The bio-functionalization and thio-phosphorylation on QCM was done on an AT-cut quartz crystal with 10 MHz resonance frequency with the same concentrations as kept for MIS and SPR measurements. The QCM was under quasi static conditions where flow was introduced manually using syringe while injection of solutions at each step in a cell as described in the supplementary information.

Results and Discussion

MIS analysis

Figure 2(a) shows the change in the gate voltage, ΔV_g, upon treatment of immobilised MBP with PKC-α kinase (4 units), its activator and ATP-S, at different time intervals. As the time interval for the interaction of MBP with PKC is extended, the changes in V_g increase until they stabilise after 10 min to a value of 12-13.5 mV. Tests conducted with ATP instead of ATP-S also revealed similar values of voltage shifts between 12-13 mV. Experiments without PKC-α showed ≤ 4 mV shift, implying that kinase activator is essential to induce phosphorylation of MBP. The reaction where inhibitor was used showed ≤ 3.7 mV. Upon addition of phosphate group to the immobilized proteins there is a negative charge imparted on the surface of the sensor (Au surface), which is responsible for the shift in the voltage across the MIS capacitor. Slight variations in the voltage that are observed in the control reactions are ascribed to the equilibrium changes in the buffer solution upon addition of kinase. To validate phosphorylation, we added AuNPs to the reaction as gold covalently attaches to the thiol groups. After adding AuNPs, a significant shift in the voltage of -18 mV was observed in the thio-phosphorylated samples. This is attributed to the fact that the AuNPs were covalently grafted to the thio-phosphorylated proteins, thereby masking the negative charge imparted by the thio-phosphoryl groups. All other experiments showed changes of less than ±5 mV. For instance, the reactions occurred in the presence of inhibitor and in the absence of kinase activator showed less than ±1.5 mV of change. These small changes are due to non-specific interactions of the gold-nanoparticles with the protein. In the reaction where phosphorylation was carried in the presence of ATP, the AuNPs interacts slightly more than the other controls due to an apparent affinity of AuNPs to any charged molecules (phosphoryl groups transferred to the protein in this case). Most of these reactions have non-specific electrostatic interactions and are removed by stringent rinsing, leaving only the

covalent bound or very strong electrostatically bound AuNPs on the surface (Star et al. 2003; Whaley et al. 2000). The successful detection of the protein phosphorylation event was then assessed to study the kinase activity. The gold surface immobilized with MBP was reacted with different concentrations of PKC-α in the presence of ATP-S and kinase activator. Figure 2(b) shows ΔV_g after maximum kinase activity was observed with different kinase concentrations. It depicts that more than 1 unit of kinase per reaction (per 100 µl) is required to see any distinguishable change from the controls.

Plasmonic coupling analysis

Upon attachment of a AuNP to the thio-phosphorylated proteins, a AuNP-Au film plasmonic couple is formed. When two plasmonic materials (in this instance Au) are brought into proximity, there is a shift in the resonance wavelength of the substrate dependent on their separation due to coupling of the respective plasmons. This arrangement of plasmonic materials is known as plasmonic ruler (Liu et al. 2011). The effect is theoretically and experimentally well understood from nanometer to angstrom distances for Au-AuNP (surface plasmon and localized surface plasmon coupling) and AuNP-AuNP (two localized plasmons pairs) couples (Davis et al. 2012; Hammond et al. 2014; Hill et al. 2012b; Kwon 2013; Su and Liu 2011; Tabor et al. 2009; Turek et al. 2012). Figure 3(a) shows the resonance signals from the samples with thio-phosphorylation and its controls. The thio-phosphorylated samples give higher absorbance than the control reactions due to attachment of nanoparticles. The variable absorbance that is seen in the controls is due to the non-specific attachment of AuNPs to the proteins. Figure 3(b) shows the statistical data on red shifts of LSPR obtained from replicates of experiments done to reproduce the experiments (n=3).

Shifts in the wavelength were seen only in the thio-phosphorylated reactions. An average red shift of around 6 nm was observed in the thio-phosphorylated samples, as compared to a small red shift, ≤ 1.5 nm, in the controls (figure 3). This large wavelength shift from the thio-phosphorylated reactions is due to the strongly enhanced electric near-field localized at the nanoparticle surface, across the whole NP surface in a periodic manner, which becomes coupled to the surface plasmon polaritons from the Au film resulting in the wavelength red shift (Mock et al. 2008). The surface distribution of the non-specifically attached AuNPs is non-periodic and therefore the shift is minute. Interestingly, a blue shift of 9.1 nm was observed in the thio-phosphorylated reaction upon stringent washing of the substrate with the reaction buffer (supplementary figure S3a). In addition, the absorbance values of all the controls were found to be consistent and much lower than for the thio-phosphorylated

reaction (supplementary figure S3b). While there was a removal of non-specifically attached AuNPs from the controls, there was also a reduction of AuNPs from the thio-phosphorylated sample. AuNPs usually have a tendency to cluster; the NP aggregation around the covalently bound AuNPs was removed upon washing. The presence of higher absorbance signal (supplementary figure S3b) is an evidence of non-removal of covalently attached AuNPs from the thio-phosphorylated proteins. An evaluation to cross validate the removal of only aggregated AuNPs was done by comparing the full width at half maximum (FWHM) of the curves before and after washing. The decrease/increase in the FWHM along with changes in the absorbance is associated with the size of the plasmonic object. A broader peak indicates the presence of large range in size and shape (disorder in distribution) of the particles. The decrease in the absolute absorbance indicates a decrease in its size distribution (Blaber et al. 2011). The FWHM of thio-phosphorylated samples decreases approximately by 30 nm after washing which is assigned to the decrease in the size of the plasmonic object (aggregated AuNPs), therefore asserting the fact that aggregated AuNPs are removed.

To visualize the electric field distribution in the plasmonic coupled system, finite element analysis using COMSOL was done as shown in Figure 4. Analysis of electric field distribution revealed a much smaller decay length of plasmons on the sensor surface than that on the AuNP (see supplementary information). Another interesting observation was that, by changing the decay constant in the empirical plasmonic ruler equation (Jain et al. 2007a) for a particle pair, the distance between the nanoparticle and the sensor film is estimated as 5±0.2 nm. This value is calculated for a particle of 20 nm with a decay constant of 0.12 that yields 5 to 6.5 nm of $\Delta\lambda$-shift on the LSPR signal (see supplementary information for details). This is in agreement with the approximate length of the bio-complex structure evaluated as 5 nm (1.5 nm for the MUA+EDC/NHS self-assembled monolayer and 3-4 nm for the protein). In the literature, Au NP-Au film coupling (Hill et al. 2012a; Mock et al. 2008) has been demonstrated with total internal reflection (TIR) illumination and dark field illumination excitation of plasmons. In our system the plasmons are excited in the reflection mode of the LSPR setup as demonstrated by Hammond et al. (2014), where plasmons are excited using white light perpendicular to the axis of the film. When plasmons are excited in this manner, the emitted intensity is also detected perpendicular to the axis of film therefore the system involves more losses due to scattering of light in comparison to TIR and dark field illumination excitation of plasmons. This is primarily why the exact models for Au NP-Au

film couples used in Hill et al. (2012b) and Mock et al. (2008) cannot be applied to our system.

SPR and QCM

Figure 5 shows the real time SPR evaluation of all the steps performed to complete the assay. The only step that is not shown is the formation of self-assembled monolayer (SAM) using mercaptoundecanoic acid (MUA) and mercaptohexanol (MCH) along with its activation by EDC/NHS (ethyl-dimethylaminopropyl carbodiimide / N-Hydroxysuccinimide). A change of 1 µRIU on the instrument is approximately equivalent to a change of 1 pg mm^{-2} protein surface coverage. MBP (19 kDa) upon binding on the surface of the gold revealed a change of 393 µRIU, which corresponds to approximately 0.002 nmol cm^{-2} or 1.24×10^{9} molecules cm^{-2} of protein surface coverage. Similarly, after phosphorylation of proteins (i.e. addition of PO_3S^-, 111.04 Da) there was an addition of 0.075 nmol cm^{-2} or 4.52×10^{10} molecules cm^{-2}. The total number of sites available for thio-phosphorylation of MBP depends upon the number of amino acids capable of becoming phosphorylated (approximately 80 serine and threonine amino acids in the case of MBP). This roughly means that around 9.92×10^{10} sites are available for thio-phosphorylation, thus implying that 45.6% were thio-phosphorylated. In the presence of inhibitor there is an insignificant shift of 3.5 µRIU. However, binding of AuNPs to the thio-phosphorylated sites yielded an average shift of 4999 µRIU, thereby, enhancing the sensitivity approximately 57 times as compared to 86.6 µRIU change observed after addition of thio-phosphoryl groups. This effect is mainly because of the mass changes happening on the surface of the sensor upon AuNPs attachment that changes the refractive index of the bio-complex (He et al. 2014). In addition, seemingly, plasmonic coupling also contributes to the enhancement of the signal in the angle resolved mode of SPR measurement (Chen et al. 2004; Jain et al. 2007b). Some non-specific attachment of the AuNPs in case of inhibition reaction was also observed that corresponded to a change of 316 µRIU. This is 15 times lower than the signal expected for AuNPs to attach and therefore it is considered insignificant.

For nanoparticle quantification, the QCM technique was implemented to calculate the total mass bound on the surface. A change of 170 Hz was observed upon AuNP addition (see supplementary information). Using the Sauerbrey equation as an approximation of the mass loading (i.e. ignoring changes in viscosity in the system), this corresponds to an estimated NP mass of 480 ng cm^{-2} or 1.45×10^{9} NPs cm^{-2} for 20 nm diameter AuNPs. This value is 10 times lower than the amount of thio-phosphoryl groups estimated by SPR. Since the size of the

nanoparticle is significantly larger than the size of the thiol group, not all phosphorylated sites are available for NP attachment. However, this would mean that either the Sauerbrey equation has overestimated the mass of the AuNPs or/and the nanoparticles are clustered. Since the NPs are suspended in a buffer, liquid entrapped could form a viscoelastic film that can cause addition damping of the quartz oscillator leading to an overestimation of the mass by 10-20%.

Conclusion

In summary, our investigation successfully demonstrates the detection of phosphorylation of proteins using AuNPs on MIS by formation of a plasmonic ruler. By using plasmonic ruler equations we estimated the distance between the AuNP and the film, which was found approximately equal to the expected SAM-protein bio-complex. We demonstrated the use of plasmonic coupling effect in detecting a bio-chemical process, protein phosphorylation. The combination of LSPR with MIS by the use of AuNPs is a simple example of how multiple techniques can merge to validate reactions. Both techniques exhibit good resolution, high sensitivity, specificity and practical applicability. Moreover the results from SPR and QCM quantified an approximate amount of protein surface coverage, thio-phosphoryl surface coverage and amount of nanoparticles on the sensor surface. Such data helps optimize reaction parameters such as concentrations of protein, ATP, kinase and nanoparticles for a complete detection of phosphorylation of proteins on an electronic platform. Although phosphorylation of MBP by PKC-α was used as a case study, this approach can be extended for assessing activity of other protein kinases. A potential application of this work would be the development of field-effect arrays where a wide range of novel kinase inhibitors could be tested.

References

Abeliovich, A., 2014. Neurological disorders: Quality-control pathway unlocked. Nature 510(7503), 44-45.

Bhalla, N., Di Lorenzo, M., Pula, G., Estrela, P., 2014. Protein phosphorylation analysis based on proton release detection: potential tools for drug discovery. Biosensor and Bioelectronics 54, 109-114.

Bhalla, N., Di Lorenzo, M., Pula, G., Estrela, P., 2015. Protein phosphorylation detection using dual-mode field-effect devices and nanoplasmonic sensors. Scientific Reports 5, 8687.

Blaber, M.G., Henry, A.-I., Bingham, J.M., Schatz, G.C., Van Duyne, R.P., 2011. LSPR imaging of silver triangular nanoprisms: correlating scattering with structure using electrodynamics for plasmon lifetime analysis. The Journal of Physical Chemistry C 116(1), 393-403.

Buee, L., Bussiere, T., Buee-Scherrer, V., Delacourte, A., Hof, P.R., 2000. Tau protein isoforms, phosphorylation and role in neurodegenerative disorders. Brain research. Brain research reviews 33(1), 95-130.

Chakraborty, P.K., Zhang, Y., Coomes, A.S., Kim, W.J., Stupay, R., Lynch, L.D., Atkinson, T., Kim, J.I., Nie, Z., Daaka, Y., 2014. G protein-coupled receptor kinase GRK5 phosphorylates moesin and regulates metastasis in prostate cancer. Cancer Research 74(13), 3489-3500.

Chen, S.J., Chien, F.C., Lin, G.Y., Lee, K.C., 2004. Enhancement of the resolution of surface plasmon resonance biosensors by control of the size and distribution of nanoparticles. Opt Lett 29(12), 1390-1392.

Cohen, P., 1988. Review Lecture: Protein Phosphorylation and Hormone Action. Proceedings of the Royal society of London. Series B. Biological sciences 234(1275), 115-144.

Cohen, P., 2002. Protein kinases--the major drug targets of the twenty-first century? Nature reviews. Drug discovery 1(4), 309-315.

Davis, T.J., Hentschel, M., Liu, N., Giessen, H., 2012. Analytical model of the three-dimensional plasmonic ruler. Acs Nano 6(2), 1291-1298.

De Laat, P., Rodenburg, R., Smeitink, J., 2014. Mitochondrial Oxidative Phosphorylation Disorders. Physician's Guide to the Diagnosis, Treatment, and Follow-Up of Inherited Metabolic Diseases, 337-359.

Hammond, J.L., Bhalla, N., Rafiee, S.D., Estrela, P., 2014. Localized Surface Plasmon Resonance as a Biosensing Platform for Developing Countries. Biosensors 4(2), 172-188.

He, P., Liu, L., Qiao, W., Zhang, S., 2014. Ultrasensitive detection of thrombin using surface plasmon resonance and quartz crystal microbalance sensors by aptamer-based rolling circle amplification and nanoparticle signal enhancement. Chemical Communication 50(12), 1481-1484.

Hill, R.T., Mock, J.J., Hucknall, A., Wolter, S.D., Jokerst, N.M., Smith, D.R., Chilkoti, A., 2012a. Plasmon Ruler with Angstrom Length Resolution. ACS Nano 6(10), 9237-9246.

Honda, H., Oda, H., Nakamoto, T., Honda, Z., Sakai, R., Suzuki, T., Saito, T., Nakamura, K., Nakao, K., Ishikawa, T., Katsuki, M., Yazaki, Y., Hirai, H., 1998. Cardiovascular anomaly, impaired actin bundling and resistance to Src-induced transformation in mice lacking p130Cas. Nature Genetics 19(4), 361-365.

Jain, P.K., Huang, W.Y., El-Sayed, M.A., 2007a. On the universal scaling behavior of the distance decay of plasmon coupling in metal nanoparticle pairs: A plasmon ruler equation. Nano Letters 7(7), 2080-2088.

Jain, P.K., Huang, X., El-Sayed, I.H., El-Sayad, M.A., 2007b. Review of some interesting surface plasmon resonance-enhanced properties of noble metal nanoparticles and their applications to biosystems. Plasmonics 2(3), 107-118.

Kerman, K., Chikae, M., Yamamura, S., Tamiya, E., 2007. Gold nanoparticle-based electrochemical detection of protein phosphorylation. Anal Chim Acta 588(1), 26-33.

Kerman, K., Kraatz, H.B., 2009. Electrochemical detection of protein tyrosine kinase-catalysed phosphorylation using gold nanoparticles. Biosensor and Bioelectronics 24(5), 1484-1489.

Kerman, K., Song, H., Duncan, J.S., Litchfield, D.W., Kraatz, H.B., 2008. Peptide biosensors for the electrochemical measurement of protein kinase activity. Analytical Chemistry 80(24), 9395-9401.

Kwon, S.H., 2013. Plasmonic Ruler With Angstrom Distance Resolution Based on Double Metal Blocks. IEEE Photonics Technology Letters 25(16), 1619-1622.

Kyriakis, J.M., 2014. In the Beginning, There Was Protein Phosphorylation. Journal of Biological Chemistry 289(14), 9460-9462.

Li, T., Liu, D., Wang, Z., 2010. Screening kinase inhibitors with a microarray-based fluorescent and resonance light scattering assay. Analytical Chemistry 82(7), 3067-3072.

Lindsay, S., 2012. Biochemistry and semiconductor electronics—the next big hit for silicon? Journal of Physics: Condensed Matter 24(16), 164201.

Liu, N., Hentschel, M., Weiss, T., Alivisatos, A.P., Giessen, H., 2011. Three-dimensional plasmon rulers. Science 332(6036), 1407-1410.

Liu, P.S., Wang, J.L., Tong, L.Y., Tao, Y.J., 2014. Advances in the Fabrication Processes and Applications of Wafer Level Packaging. Journal of Electronic Packaging 136(2), 024002.

Liu, Q., Molkentin, J.D., 2011. Protein kinase Calpha as a heart failure therapeutic target. Journal of molecular and cellular cardiology 51(4), 474-478.

Mock, J.J., Hill, R.T., Degiron, A., Zauscher, S., Chilkoti, A., Smith, D.R., 2008. Distance-dependent plasmon resonant coupling between a gold nanoparticle and gold film. Nano Letters 8(8), 2245-2252.

Morgan, E., Varro, R., Sepulveda, H., Ember, J.A., Apgar, J., Wilson, J., Lowe, L., Chen, R., Shivraj, L., Agadir, A., Campos, R., Ernst, D., Gaur, A., 2004. Cytometric bead array: a multiplexed assay platform with applications in various areas of biology. Clinical Immunology 110(3), 252-266.

Noble, M.E.M., Endicott, J.A., Johnson, L.N., 2004. Protein kinase inhibitors: Insights into drug design from structure. Science 303(5665), 1800-1805.

Overington, J.P., Al-Lazikani, B., Hopkins, A.L., 2006. How many drug targets are there? Nature reviews Drug discovery 5(12), 993-996.

Rusinova, R., Shen, Y.M., Dolios, G., Padovan, J., Yang, H., Kirchberger, M., Wang, R., Logothetis, D.E., 2009. Mass spectrometric analysis reveals a functionally important PKA phosphorylation site in a Kir3 channel subunit. Pflugers Archiv : European journal of physiology 458(2), 303-314.

Star, A., Gabriel, J.C.P., Bradley, K., Gruner, G., 2003. Electronic detection of specific protein binding using nanotube FET devices. Nano Letters 3(4), 459-463.

Steen, H., Jebanathirajah, J.A., Springer, M., Kirschner, M.W., 2005. Stable isotope-free relative and absolute quantitation of protein phosphorylation stoichiometry by MS. Proceedings of National Academy of Sciences USA 102(11), 3948-3953.

Su, X., Liu, X., 2011. The plasmonic ruler goes 3D! Chemphyschem 12(15), 2707-2708.

Tabor, C., Murali, R., Mahmoud, M., El-Sayed, M.A., 2009. On the use of plasmonic nanoparticle pairs as a plasmon ruler: the dependence of the near-field dipole plasmon

coupling on nanoparticle size and shape. Journal of Physical Chemistry A 113(10), 1946-1953.

Turek, V.A., Cecchini, M.P., Paget, J., Kucernak, A.R., Kornyshev, A.A., Edel, J.B., 2012. Plasmonic ruler at the liquid-liquid interface. ACS Nano 6(9), 7789-7799.

Viatour, P., Merville, M.P., Bours, V., Chariot, A., 2005. Phosphorylation of NF-kappaB and IkappaB proteins: implications in cancer and inflammation. Trends Biochem Sci 30(1), 43-52.

Weller, M., 1979. Protein phosphorylation. Pion Ltd.

Whaley, S.R., English, D.S., Hu, E.L., Barbara, P.F., Belcher, A.M., 2000. Selection of peptides with semiconductor binding specificity for directed nanocrystal assembly. Nature 405(6787), 665-668.

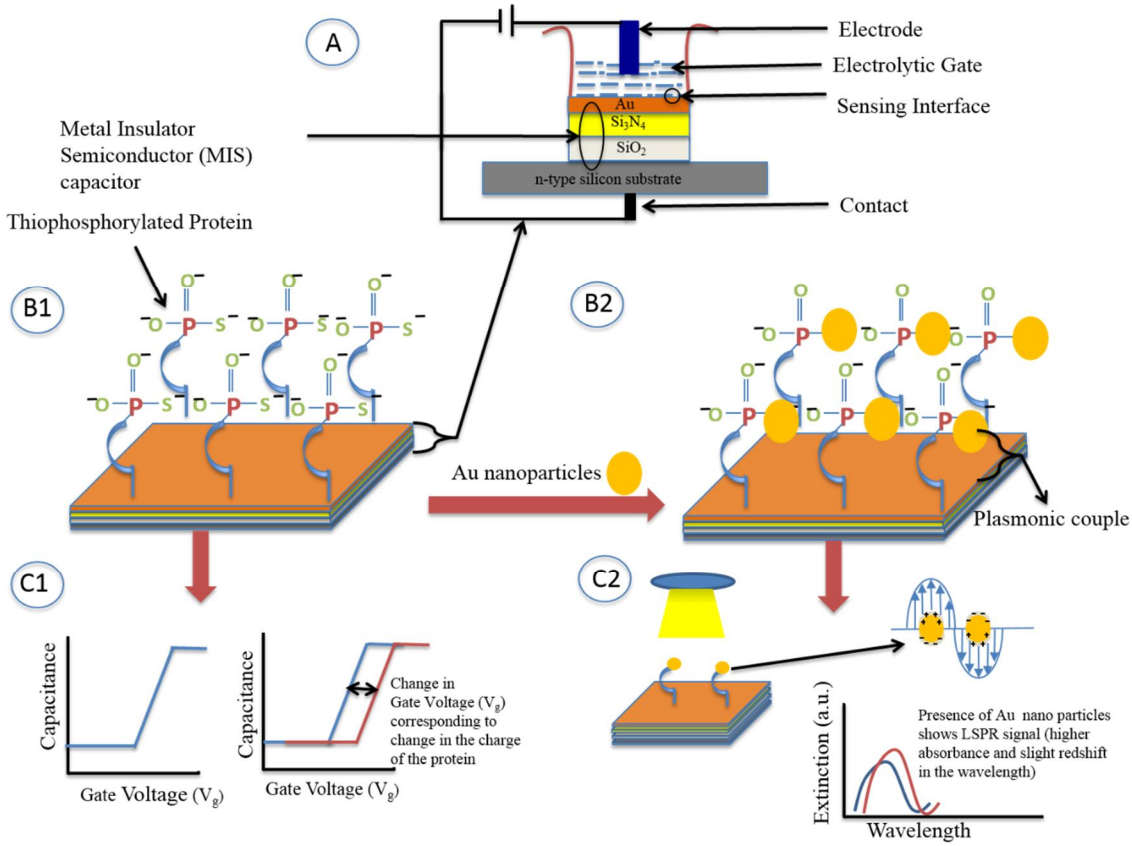

Figure 1: Scheme for protein phosphorylation analysis: (A) Field effect device well for protein phosphorylation measurement; (B1) metal insulator semiconductor (MIS) capacitor structure with immobilized proteins after thio-phosphorylation; (B2) AuNPs attached to the thiol groups of thio-phosphorylated protein in plasmonic ruler configuration; (C1) Capacitance vs. gate voltage characteristics curve of MIS and change in gate voltage corresponding to the charge on the phosphorylated proteins; (C2) LSPR measurement of plasmonic ruler.

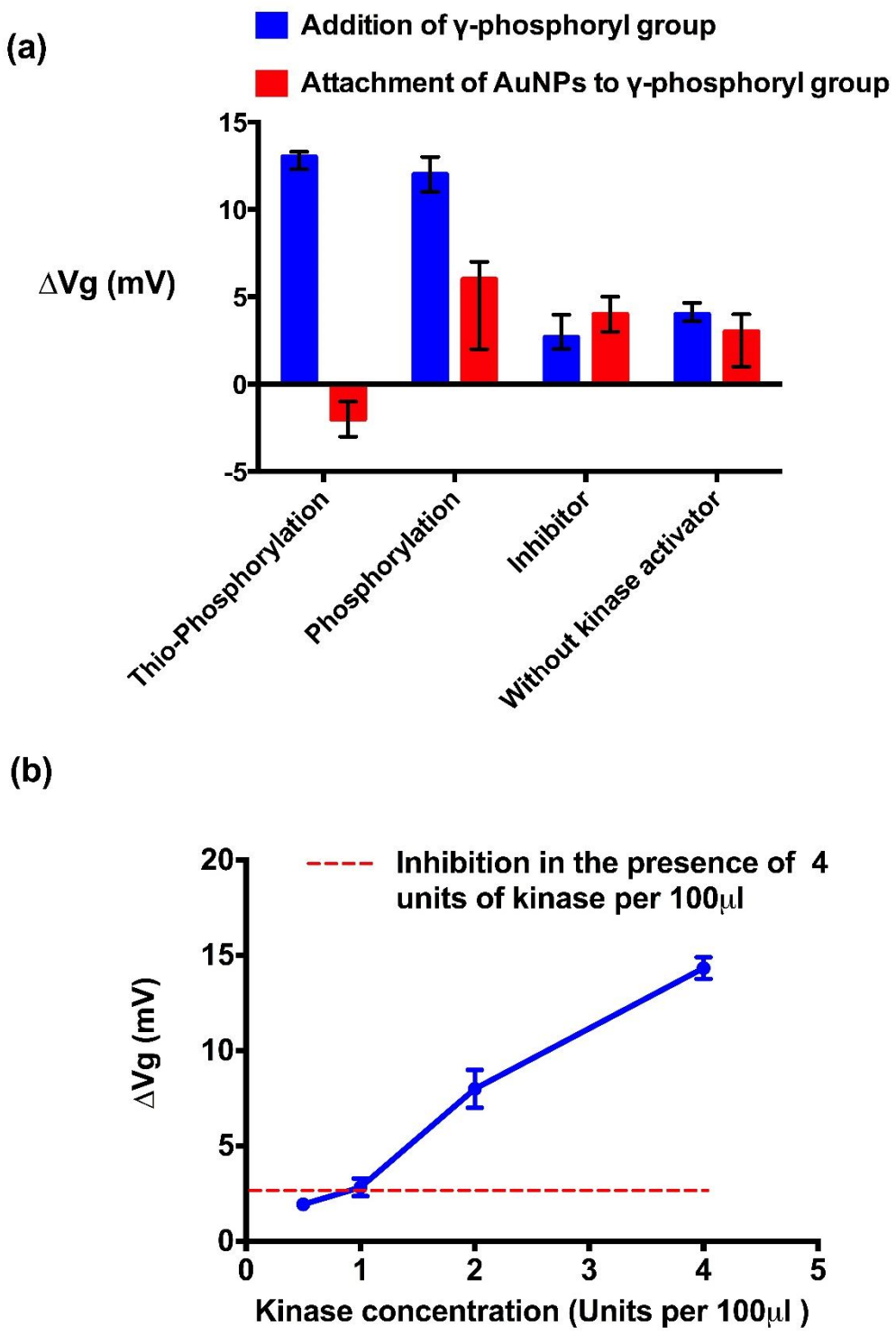

Figure 2: Protein Phosphorylation on Au.: (a) changes in gate potential upon thio-phosphorylation of MBP by PKC-α kinase in the presence of ATP-S, phosphorylation of MBP by PKC-α kinase in the presence of ATP and control reactions in the absence of kinase activator & in the presence of kinase inhibitor; (b) Variations in V_g observed upon thio-phosphorylation with different kinase concentrations

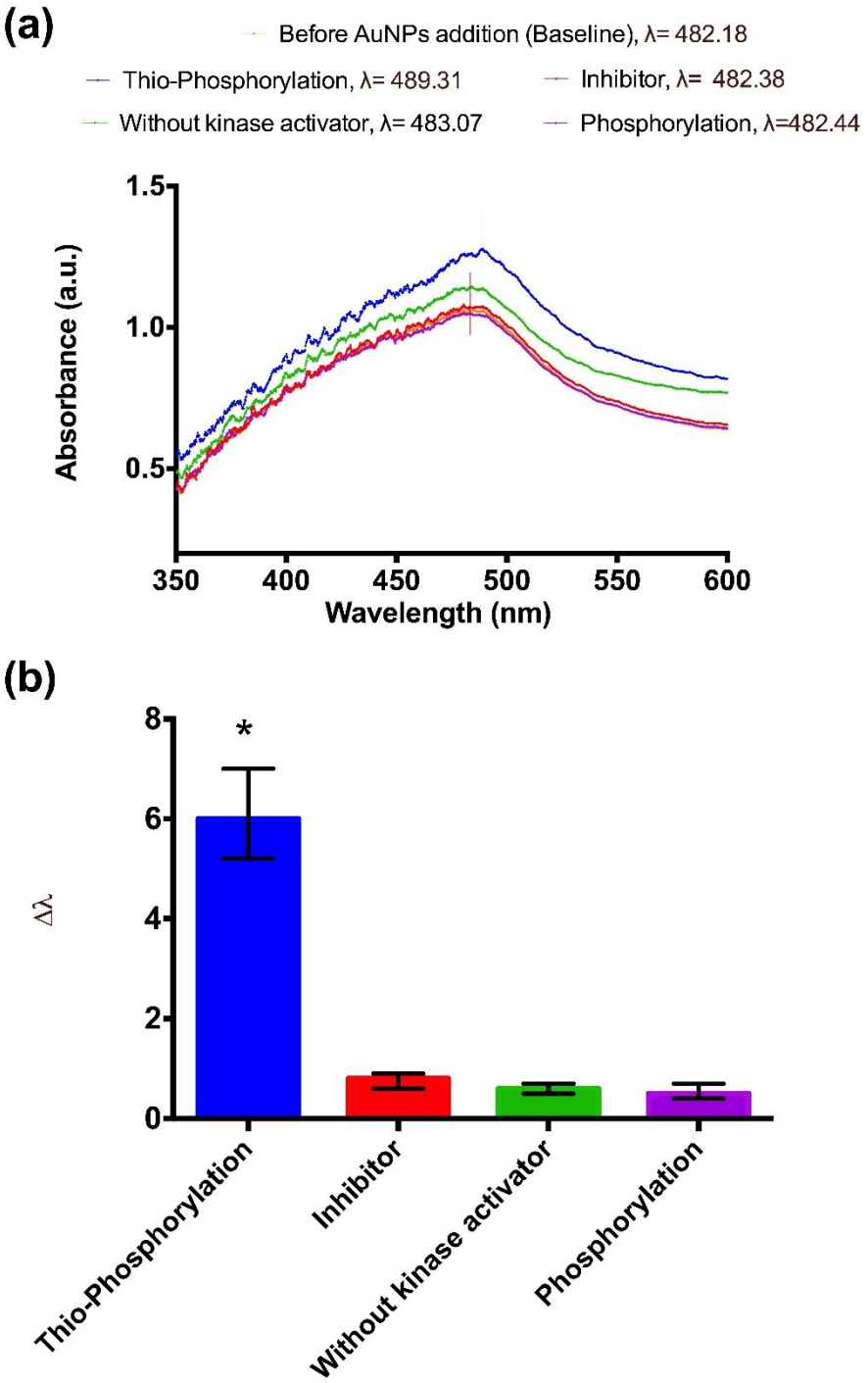

Figure 3: LSPR measurements for protein phosphorylation (a) LSPR characteristic curve for Au surface with immobilized proteins (baseline) thio-phosphorylation, phosphorylation, and controls in absence of kinase activator and presence of kinase inhibitor – the vertical lines indicate the position of the peaks before and after thio-phosphorylation; (b) LSPR wavelength shift of the spectra peaks with respect to the baseline spectrum (Au surface with immobilized protein) after adding AuNPs to thio-phosphorylated, phosphorylated and control reaction samples.

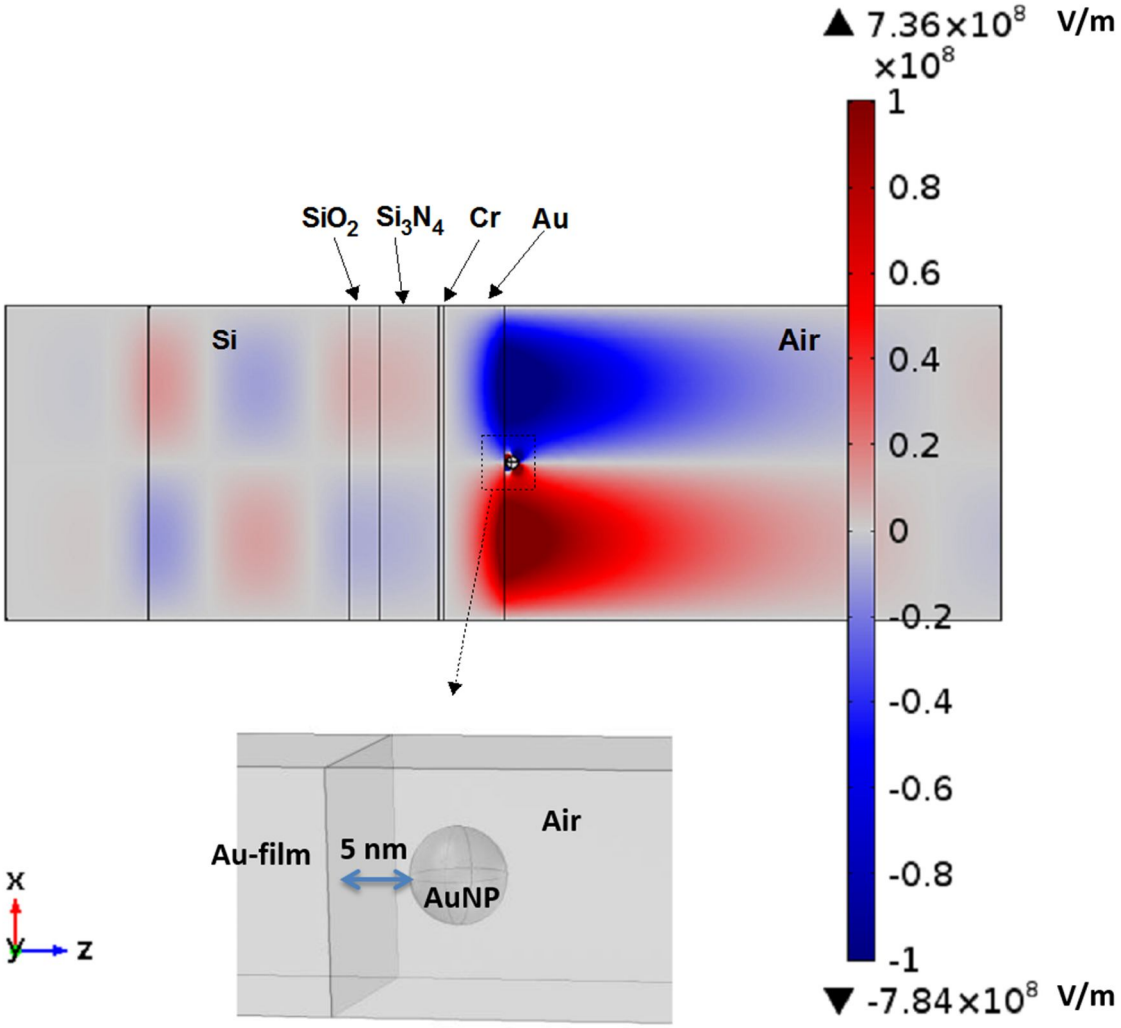

Figure 4: COMSOL simulation for plasmonic coupling showing electric field distribution of plasmonic ruler in AuNP-Au film coupled pair.

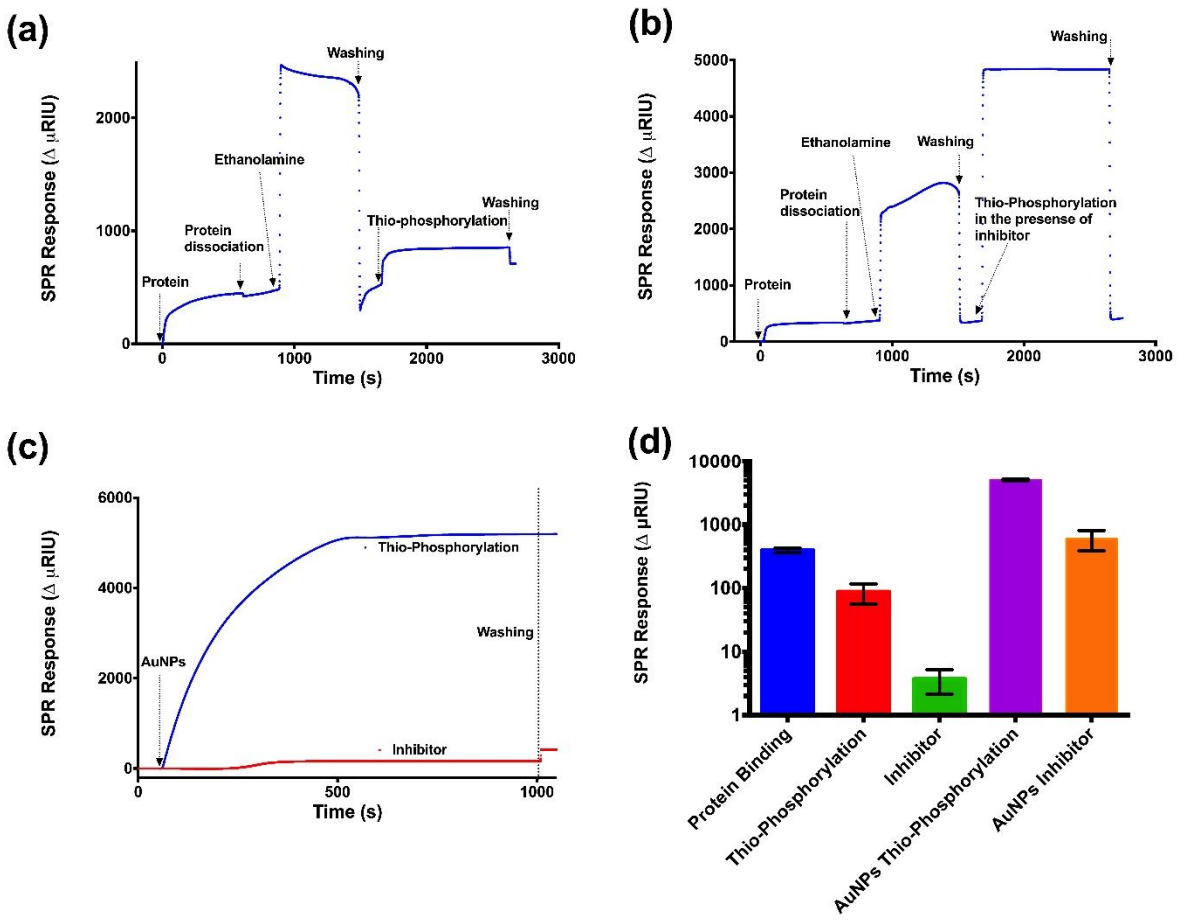

Figure 5: SPR measurements (a) real time response for thio-phosphorylation reaction; (b) real time response in the presence of inhibitor; (c) AuNP attachment to thio-phosphorylated (blue curve) and inhibition reaction (red); (d) SPR response statistics for n=3 samples.